



Simulation of κ -Carbide Precipitation Kinetics in Aged Low-Density Fe–Mn–Al–C Steels and Its Effects on Strengthening

Jaeun Lee¹ · Siwook Park¹ · Hwangsun Kim¹ · Seong-Jun Park² · Keunho Lee³ · Mi-Young Kim¹ · Phaniraj P. Madakashira¹ · Heung Nam Han¹

Received: 10 November 2017 / Accepted: 20 December 2017 / Published online: 12 March 2018
© The Korean Institute of Metals and Materials 2018

Abstract

Fe–Al–Mn–C alloy systems are low-density austenite-based steels that show excellent mechanical properties. After aging such steels at adequate temperatures for adequate time, nano-scale precipitates such as κ -carbide form, which have profound effects on the mechanical properties. Therefore, it is important to predict the amount and size of the generated κ -carbide precipitates in order to control the mechanical properties of low-density steels. In this study, the microstructure and mechanical properties of aged low-density austenitic steel were characterized. Thermo-kinetic simulations of the aging process were used to predict the size and phase fraction of κ -carbide after different aging periods, and these results were validated by comparison with experimental data derived from dark-field transmission electron microscopy images. Based on these results, models for precipitation strengthening based on different mechanisms were assessed. The measured increase in the strength of aged specimens was compared with that calculated from the models to determine the exact precipitation strengthening mechanism.

Keywords Low-density steel · Aging · κ -Carbide · Precipitation · Numerical simulation

1 Introduction

In order to reduce greenhouse gas emissions and improve energy efficiency, there is a growing demand for weight reduction in transportation systems, e.g. in automotive and defense sectors. Current research in the steel industry is focusing on reducing the density of steel while maintaining high strength and elongation to develop alloys suitable for automotive applications. This has led to the development of several types of lightweight steels with excellent specific strength (strength-to-weight ratio) and ductility [1–12].

Lightweight steels can be classified into ferritic, austenitic, and multiphase steels, depending on their constituent phases; austenitic steels based on the Fe–Al–Mn–C system have higher Mn and Al contents than ferritic steels, excellent mechanical properties, and high weight reduction rates [2, 13–15]. The most effective strengthening mechanism in these austenitic low-density steels is precipitation hardening due to the (Fe, Mn)₃AlC perovskite κ -carbide phase [16–18]. Nano-scale κ precipitates are known to increase both the yield strength and tensile strength in steels to > 1 GPa. Therefore, the use of the austenite phase and κ precipitates is an effective way to improve the mechanical performance of low-density steels.

Age hardening in austenitic Fe–Mn–Al–C steels, which is closely related to the formation of κ -precipitates, has been the subject of a number of recent studies [1, 2, 19–29]. Kalashnikov et al. [1] reported that an optimal combination of mechanical properties could be achieved for steels containing 9–9.5 wt% Al, 0.9–0.95 wt% C, and 28.5–30.5 wt% Mn. This hardening was attributed to coherency strains produced by spinodal decomposition in the early stage of aging [20, 21] and also coherent κ -carbide precipitation in austenite [30, 31]. During aging, intragranular carbide precipitation initially occurs, followed by precipitation along

✉ Heung Nam Han
hnhhan@snu.ac.kr

¹ Department of Materials Science and Engineering and Research Institute of Advanced Materials, Seoul National University, 1 Gwanak-ro, Gwanak-gu, Seoul 08826, Republic of Korea

² Advanced Metallic Materials Division, Ferrous Alloy Department, Korea Institute of Materials Science, 797 Changwondae-ro, Seongsan-gu, Changwon, Gyeongnam 51508, Republic of Korea

³ Agency for Defense Development, P.O. Box 35-9, Yuseonggu, Daejeon 34075, Republic of Korea

grain boundaries [32, 33]. Changes in the mechanical properties with different aging times have been reported in the literature. However, quantitative analysis of the correlation between the mechanical properties and the κ -carbide volume fraction and size has not yet been thoroughly investigated. Recently, Kim et al. [34] reported increased strength due to dislocation shearing and bypassing κ -carbide precipitates in an austenitic Fe–Mn–Al–C steel with added Si and Mo. In this study, the measured strength increase was smaller than the calculated increase in strength due to the bypassing of dislocations. Therefore, they concluded that dislocation shearing of κ -carbides was the predominant mechanism for strengthening in this system.

Some studies used numerical methods to evaluate the precipitation kinetics during aging of austenitic [35, 36], ferritic [37], and martensitic [38] steels and their effects on the mechanical properties. To simulate the kinetics of ordered B2-type precipitates during aging of martensitic PH 13-8Mo steel, Povoden-Karadeniz and Kozeshnik [38] used the thermo-kinetic software MatCalc with thermodynamic databases for the B2, Fe–Al austenite, and Fe–Ni and Fe–Al binary phases. They also evaluated the increase in yield strength due to B2 precipitation by accounting for a change in the underlying mechanism from dislocation shearing to bypassing with an increase in precipitate size during aging. Holzer and Kozeshnik [37] calculated the precipitation kinetics and strengthening due to bcc and fcc copper precipitates in ferritic steels. They used the generalized broken bond (GBB) approach to calculate the energy of the precipitate/matrix interface energy, which is required in the simulation.

In the present study, we investigated the precipitation behavior of κ -carbide and its effect on the mechanical properties of Fe–Mn–Al–C steels after aging using transmission electron microscopy (TEM), Vickers indentation, and tensile tests. In addition, efforts were made to simulate the precipitation of κ -carbides from the austenite phase using MatCalc. In this simulation, a thermodynamic database for multi-component Fe–Mn–Al–C systems [39] was used as the CALPHAD method. The simulation results allowed us to describe the evolution of the size distribution and volume fraction of the carbide phase during aging. The simulation results were verified by comparing them with the results of experimental measurements. Based on the calculated data, the effect of κ -carbide on the strengthening mechanism is discussed.

2 Experimental and Simulation Methods

A low-density steel with a chemical composition of Fe–0.8C–31.52Mn–8.73Al (wt%) was used in the present work. The ingot was soaked at 1200 °C for 2 h and then

hot-rolled to a thickness of 8 mm with a final rolling temperature above 900 °C; the total thickness reduction due to hot-rolling was 90%. After hot rolling, the plate was cooled to room temperature by spraying it with water. The plate was then solution-treated at 1050 °C for 2 h, followed by water quenching. Specimens cut from the solution-treated plate were isothermally aged at 550 °C for up to 1000 min. For convenience, the specimen solution-treated at 1050 °C is referred to as ST, and the specimens aged at 550 °C for 10, 30, 100, and 1000 min are denoted as A10, A30, A100, and A1000, respectively. True stress-strain responses and corresponding strain hardening rates of the solution-treated and aged samples were investigated using tensile tests at a nominal strain rate of $1.33 \times 10^{-3} \text{ s}^{-1}$ at room temperature. Vickers microhardness measurements were performed under a load of 1 kgf.

The simulation of κ -carbide evolution during aging was performed with the thermo-kinetic software package MatCalc (version 5.30). In MatCalc, nucleation kinetics are based on classical nucleation theory [40, 41] and evolution equations for the radius and composition of the precipitate were derived from thermodynamic principles. In the simulation, the thermodynamic and kinetic data were calculated using the thermodynamic database TCFE2000 and its upgraded version [39, 42], and the MatCalc mobility database mc_fe. Austenite was chosen as the matrix phase and partial transformation of the matrix into ferrite at low temperature was not considered as precipitation of κ -carbide occurs only in the austenite phase. The dislocation density of the austenite matrix phase was taken to be 10^8 m^{-2} , similar to that of standard annealed steel [43]. The nucleation sites considered in this simulation were not only dislocations, but were grain boundaries, grain boundary edges, and grain boundary corners, which are 2-, 3-, and 4-grain junctions, respectively. Sub-grain boundaries were not included as the specimen was solution-treated at 1050 °C and such features were not observed experimentally. The parameter sets for the simulation are listed in Table 1.

Cross-sectional specimens for TEM analysis (FEI-Tecnai F20) used to verify the simulated results were prepared by cutting pieces from the austenite region using the focused ion beam (FIB; FEI-Helios 650) technique. The presence of κ -carbide and the size distribution and phase fraction of its precipitates were analyzed using dark-field TEM images of the specimens and their corresponding selected area diffraction patterns (SADP). Several dark-field TEM images were analyzed for each aging time and the total area of image analysis was about 19,000 nm² for each sample type. To calculate the volume fraction of the precipitates using dark-field TEM images, it was assumed that the area fractions from the 2D images could be extrapolated to 3D space. Since the κ -carbide is known to have a cuboid shape [19], it was assumed that the length of one side of the largest precipitate

Table 1 Parameter set for the simulations and calculations performed in this work

Phase	Parameter	Value	Source
Austenite (matrix)	Dislocation density ($/m^2$)	10^8	[43]
	Shear modulus, G_γ (GPa)	66.2	Nanoindentation ^a
	Lattice parameter, a_γ (Å)	3.675	XRD
	Burgers vector, b_γ (nm)	0.260	XRD ^b
	Grain diameter (μm)	100	EBSD
κ -carbide (precipitates)	Interfacial energy (J/m^2)	0.127	Thermodynamic database: KY201110 [39]
	Shear modulus, G_κ (GPa)	90.0	[55]
	Lattice parameter, a_κ (Å)	3.730	XRD

^aG was calculated using Young's modulus obtained from nanoindentation and ν (= 0.33)

^b2

on the dark-field image corresponded to the height. The volume fraction of the precipitates in the total image volume was determined using $\text{sum of each precipitate volume}/(\text{image width})^2 \times \text{height}$.

3 Results and Discussion

3.1 Mechanical Properties and Simulation of Precipitate Evolution

Figure 1a shows engineering stress-strain curve for the steels aged at 550 °C and Fig. 1b shows the change in yield strength, tensile strength, and elongation with aging time. The yield and tensile strength increased with aging time up to 1000 min. The Vickers hardness shown in Fig. 1c increased up to 350 HV over the time periods investigated in the present study. This increase in strength and hardness with aging time was due to the precipitation of κ -carbide. A rapid increase in hardness was observed from 30–100 min of aging. This increase in hardness indicated an acceleration of carbide precipitation after 30 min of aging.

Figure 2 shows the calculated equilibrium phase fraction for five phases (liquid, austenite, ferrite, κ -carbide, and β -Mn) in the Fe–0.8C–31.52Mn–8.73Al alloy at 200–1400 °C. At a solution treatment temperature of 1050 °C, the alloy contained austenite and ferrite phases. The austenite phase fraction decreased with decreasing temperature and became zero at 600 °C, below which ferrite was the dominant phase; the β -Mn phase was stable below 500 °C. The κ -carbide phase fraction was constant between ~ 300–600 °C, above which point it decreased as the temperature increased before fully dissolving at 850 °C. Based on these trends, the solution-treated and quenched specimen in the present study was expected to have a microstructure consisting mainly of metastable austenite and ferrite phases. At an aging temperature of 550 °C, κ -carbide is expected to

precipitate and increase in volume fraction with time to a maximum fraction of 16.5% (corresponding to the equilibrium value).

Figure 3a shows the change in the simulated phase fraction and radius of κ -carbides with time of aging at 550 °C. The carbide precipitation started early and increased significantly to 14% after 30 min of aging. After approximately 1000 min of aging, the carbide phase fraction was relatively steady at ~ 14%. This amount was slightly lower than the calculated equilibrium phase fraction of 16.5%, which indicates that precipitation was nearly complete. The simulated average precipitate size during heat treatment also increased gradually with increasing aging time.

The volume fraction and size of the precipitates in samples A100 and A1000 were measured from TEM micrographs and compared with the simulated values. Several TEM images (Fig. 3b, d) were utilized to obtain the volume fraction of the precipitates. The fraction and size of κ -carbides in A100 and A1000 were 0.07 and 1.64 ± 0.89 , and 0.16 and 3.15 ± 2.02 nm, respectively. No precipitates were observed in the dark-field TEM images of samples ST, A10, and A30. The results for precipitate fraction and size are shown in Fig. 3a as green and blue symbols, respectively, showing that the simulated phase fractions were in reasonable agreement with the measured values.

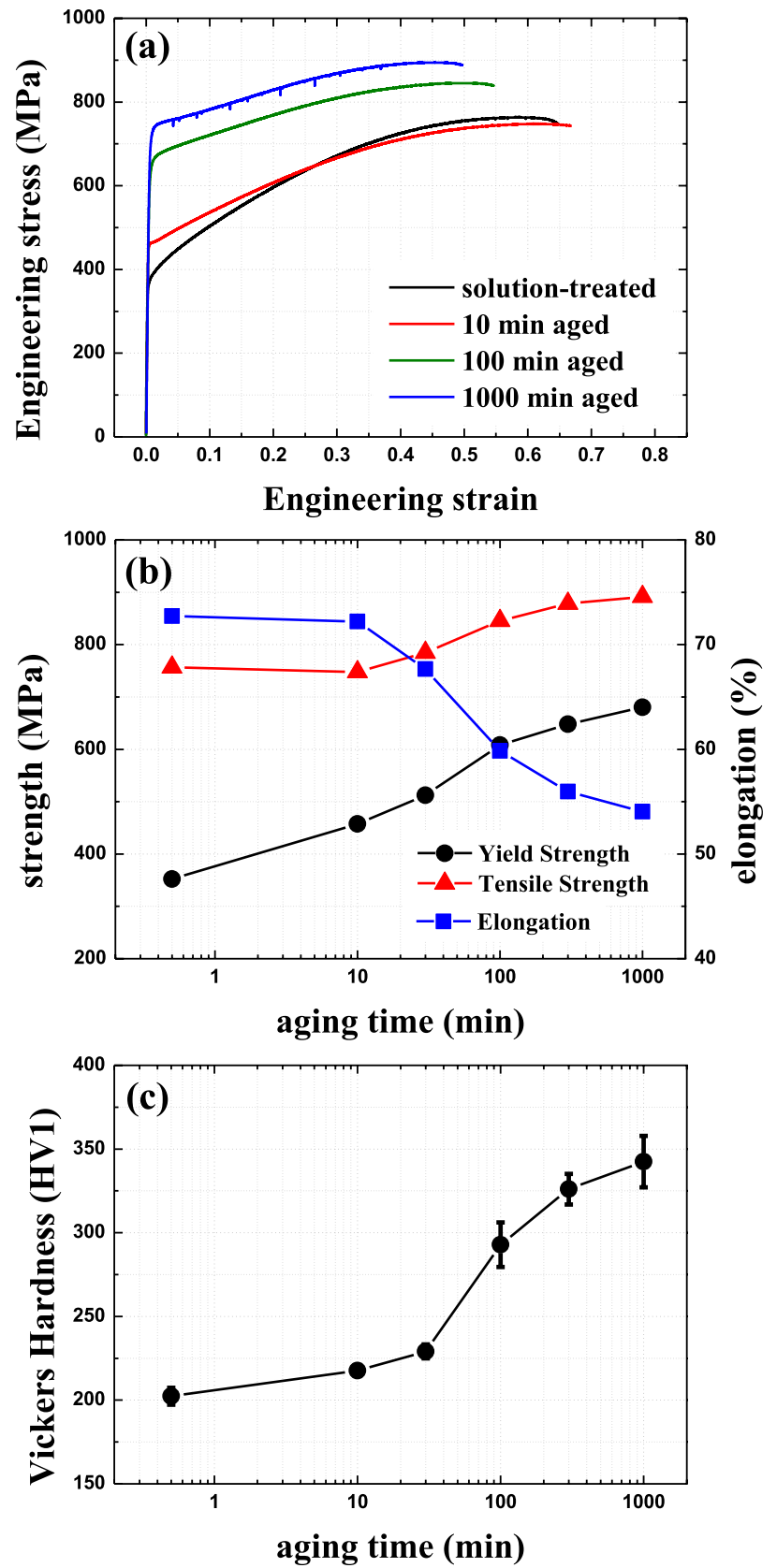
3.2 Hardening Mechanisms

Since the grain size of the steels did not change with aging time, the total yield strength of the steels can be expressed as a linear combination of the following strengthening mechanism:

$$\sigma_{ys} = \sigma_0 + \Delta\sigma_{ppt} + \Delta\sigma_{ss} \quad (1)$$

where σ_0 is the sum of Peierls stress and grain boundary strengthening, $\Delta\sigma_{ppt}$ is the precipitation hardening, and $\Delta\sigma_{ss}$ is the strengthening from solute atoms. The solid solution

Fig. 1 **a** Engineering stress-strain curves for the steels aged at 550 °C. **b** Yield strength, tensile strength, and elongation as functions of aging time. **c** Vickers hardness as a function of aging time



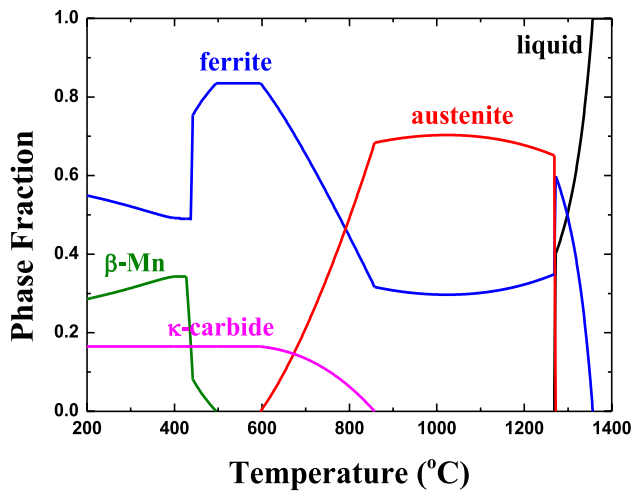


Fig. 2 Equilibrium phase fraction as a function of temperature for the Fe–0.8C–31.52Mn–8.73Al alloy calculated using the CALPHAD method [39]

strengthening by Mn, Al, and C is generally described as [44–46]:

$$\Delta\sigma_{ss} = \sum K_i c_i^n \quad (2)$$

where K_i is a strengthening coefficient for element i , c_i is a weight percent of solute atoms, and n ($= 2/3$) is a constant for concentrated solutions. $\Delta\sigma_{ss}$ was calculated using a K_i of 2.8, 0.8, and 249.6 MPa wt%⁻¹ for Mn, Al, and C, respectively [47]. As shown in Fig. 4, the weight percentages of Mn, Al, and C in austenite for each aging time were obtained from MatCalc calculations. As the aging time increased, the number of solute atoms in the matrix phase gradually decreased, especially for C due to the precipitation of κ -carbide. The decrease in yield strength due to the reduction of the solid solution was calculated from Eq. (2) as 99.1 MPa for 100 min of aging, and 194.7 MPa for 1000 min of aging (Fig. 4d).

Dislocations moving through a matrix containing precipitates can either shear the precipitates or bypass them, leaving behind a dislocation loop. Both shearing and bypassing of precipitates by dislocations result in alloy strengthening. If the precipitate is sheared, then strengthening can arise due to three mechanisms. First, order strengthening (shearing κ -carbide), which has an ordered L12 structure, results in the creation of an anti-phase boundary that requires additional energy. The second mechanism is strengthening due to coherency strain that arises from the lattice mismatch between carbide and matrix. Third, strengthening due to differences in shear modulus between the matrix and κ -carbide is also possible. The contribution to the yield strength from each mechanism can be calculated using the following equations [48]:

$$\Delta\sigma_{\text{order}} = M 0.81 \frac{\gamma_{\text{APB}}}{2b} \left(\frac{3\pi f}{8} \right)^{1/2} \quad (3)$$

$$\Delta\sigma_{\text{coh}} = M \alpha_\epsilon (G_\gamma \epsilon_c)^{3/2} \left(\frac{rf}{0.5Gb} \right)^{1/2} \quad (4)$$

$$\Delta\sigma_{\text{mod}} = M 0.0055 (\Delta G)^{3/2} \left(\frac{2f}{G} \right)^{1/2} \left(\frac{r}{b} \right)^{(3m/2)-1} \quad (5)$$

where M ($= 3.06$) is the mean orientation factor for the fcc polycrystalline matrix [49], G_γ is the shear modulus of austenite, ΔG is the shear modulus difference between austenite and κ -carbide, b is the magnitude of the Burgers vector, and α_ϵ ($= 2.6$) and m ($= 0.85$) are constants for fcc metals [48]. Here, r and f are the average radius and fraction of the precipitate, respectively and ϵ_c is the constrained lattice parameter misfit, $\epsilon_c = (2/3)\delta$, with $\delta = \Delta a/a$ as the ambient temperature lattice parameter misfit. The lattice parameter mismatch between the austenite matrix and the κ -carbide precipitate was approximately 1% based on the lattice parameters measured by XRD. γ_{APB} is the antiphase boundary energy per unit area, which is produced when the ordered κ -carbide is sheared. The parameters used in calculating the strengthening contribution are given in Table 1.

The coherency strain could be maximum at the particle interface when dislocation approaches a particle, and the force proportional to the difference in shear modulus between particle and matrix is greatest when the dislocation has entered the precipitate. Therefore, the contributions to the strength due to coherency strain ($\Delta\sigma_{\text{coh}}$) and modulus mismatch ($\Delta\sigma_{\text{mod}}$) reach their maximum when the shearing dislocation is close to the precipitate-matrix interface and intersects the precipitate, respectively. On the other hand, the maximum force exerted by a spherical particle of an ordered phase may be obtained by assuming the dislocation lies along a diameter, so that order strengthening ($\Delta\sigma_{\text{order}}$) reaches its maximum when half the precipitate is sheared by the dislocation [50]. Therefore, in the present study, the larger one of the two ($\Delta\sigma_{\text{order}}$ and $\Delta\sigma_{\text{coh}} + \Delta\sigma_{\text{mod}}$), was taken as the strengthening contribution by shearing [51].

When dislocations bypass the precipitates, the increase in strength is given by Orowan's equation [52, 53]:

$$\Delta\sigma_{\text{Orowan}} = M \frac{0.4Gb \ln(2r/b)}{\pi \lambda \sqrt{1-\nu}} \quad (6)$$

where ν ($= 0.33$) is Poisson's ratio for austenite [49] and λ is the inter-precipitate distance, which is taken as the square lattice spacing in parallel planes, as given by Nembach [54]:

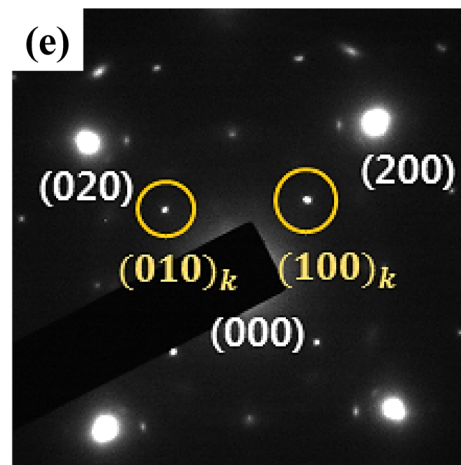
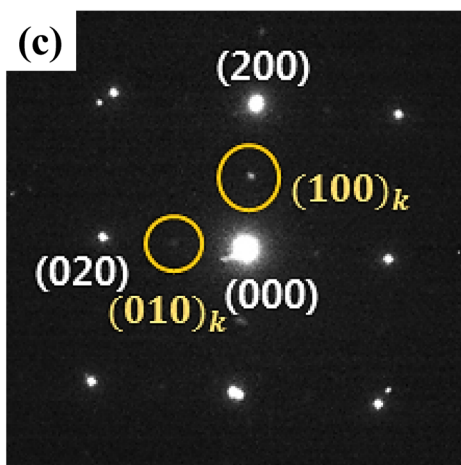
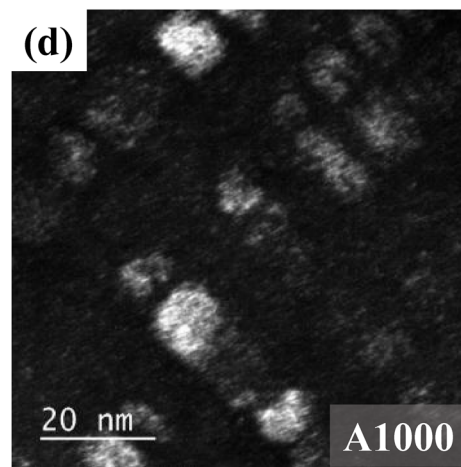
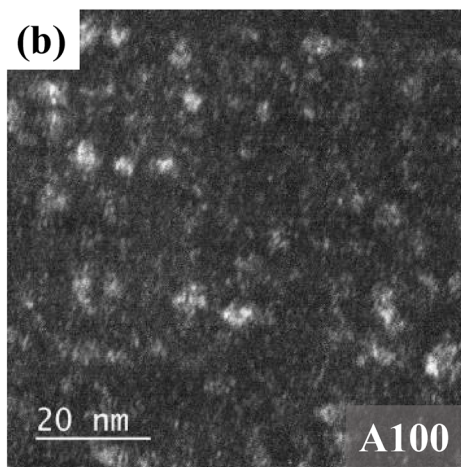
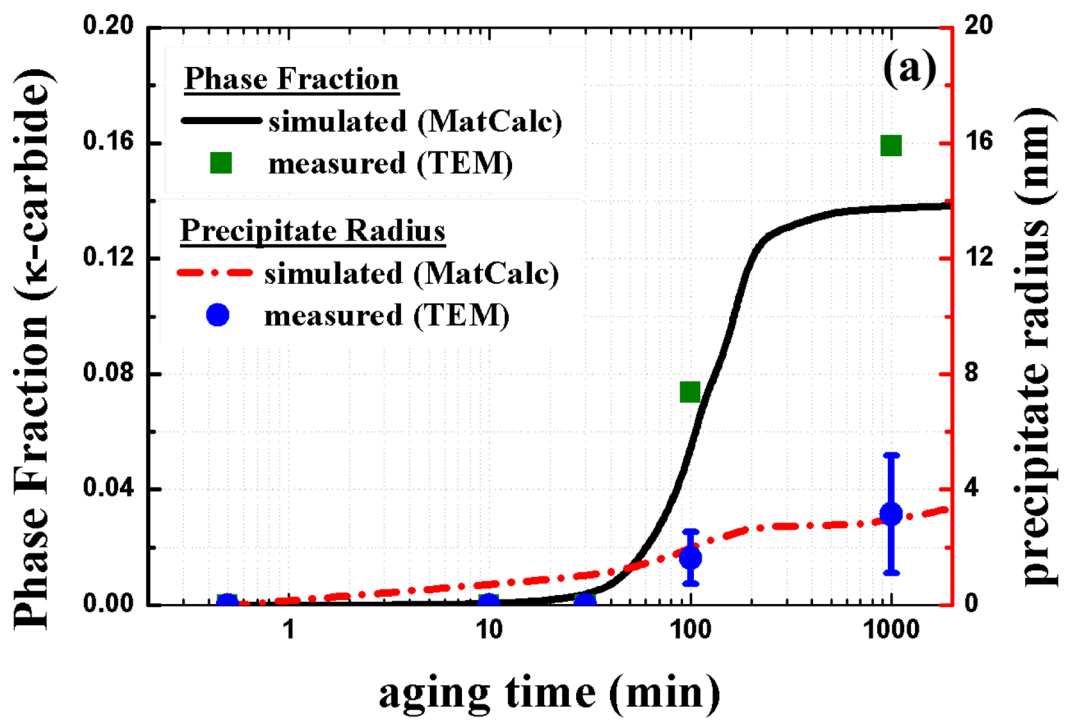


Fig. 3 **a** Predicted evolution of precipitate phase fraction and mean radius of κ -carbide (solid line) during aging at 550 °C compared with values measured from TEM micrographs (symbols). **b** Dark-field TEM image and **c** selected area diffraction pattern for $z = [001]$ of the steels aged for 100 min at 550 °C (A100). **d** Dark-field TEM image and **e** selected area diffraction patterns for $z = [001]$ of the steels aged for 1000 min at 550 °C (A1000)

$$\lambda = r \left(\sqrt{\frac{3\pi}{4f}} - 1.64 \right) \quad (7)$$

Equations (3)–(7) were used to calculate the values of $\Delta\sigma_{\text{order}}$, $\Delta\sigma_{\text{coh}} + \Delta\sigma_{\text{mod}}$, and $\Delta\sigma_{\text{Orowan}}$. The critical precipitate

radius (r^*), above which the dislocation bypass the precipitates rather than shear them, was also estimated.

When dislocations encounter arrays of obstacles, they first bend to make an angle between the obstacles. The critical angle (φ_c) at which they can bend before breaking through the barrier is determined by the type and number of obstacles [52]. The strength required for continued dislocation motion is modified by a factor of $\cos(\varphi_c/2)$ for strong obstacles. The average factor calculated for all possible angles using $(1/\pi) \int_0^\pi (\cos(\varphi_c/2)) d\varphi_c$ is 0.64. The precipitate fraction in the present study was much larger than that of normal micro-alloyed steels, and thus, a multiplication factor of 0.64 was used to calculate the precipitation strengthening. It should be noted here that Eqs. (3)–(6) were developed for

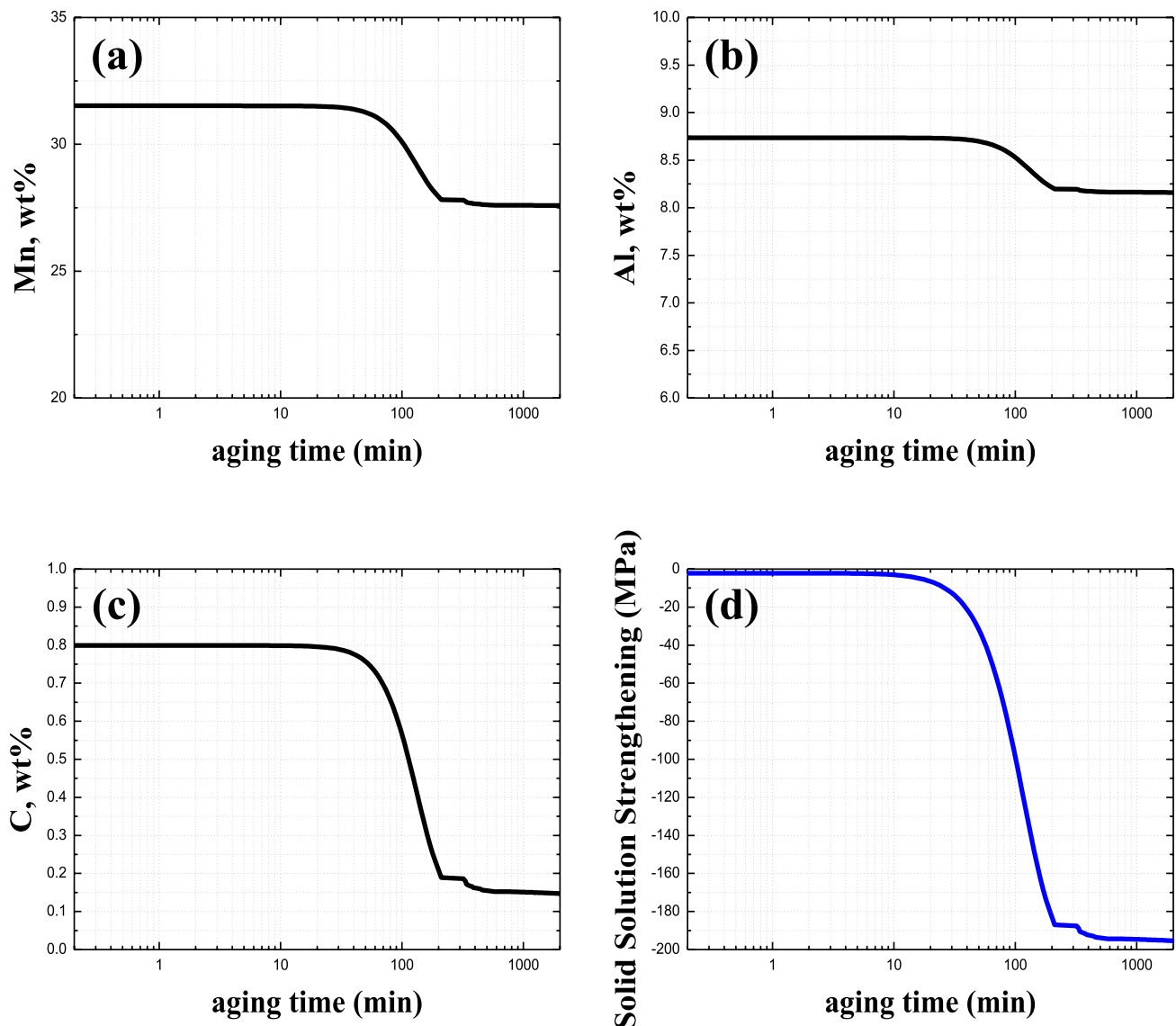


Fig. 4 Simulated variation in chemical composition (wt%) of **a** Mn, **b** Al, and **c** C in austenite according to aging time. **d** Variation in yield strength due to the reduction of the solid solution

much smaller precipitate fractions ($\sim 10^{-4}$) than occurred in the present study ($\sim 10^{-1}$).

Using the simulated results from Sect. 3.1 and Eqs. (1)–(7), the main strengthening mechanism was identified as a function of precipitate radius. Figure 5a shows the increase in strength as a function of precipitate radius after 100 min of aging using the measured volume fraction of 0.054. Here, r^* , above which strengthening by the Orowan mechanism is relevant, was predicted to be 8.02 nm. Order strengthening was the dominant mechanism below a precipitate radius of 2.72 nm, and between 2.72 and 8.02 nm the strengthening was due to coherency strain and modulus differences. The measured precipitate radius after 100 min aging was between 1.20 and 2.08 nm, which fell in the domain of order strengthening. Therefore, the strengthening observed in the specimen aged for 100 min was due to precipitate shearing with order strengthening as the dominant mechanism.

Figure 5b shows the increase in strength as a function of precipitate radius after 1000 min of aging using the measured volume fraction of 0.137. The critical precipitated radius above which strengthening by the Orowan mechanism is operative was predicted to be 9.41 nm. Order strengthening was the dominant mechanism below a precipitate radius of 2.73 nm, and the strengthening was due to coherency strain and modulus differences between 2.73 and 9.41 nm. The measured precipitate radius after 1000 min aging was between 2.14 and 4.16 nm, which was lower than the critical radius but in the region where strengthening due to all three mechanisms (order, coherency strain, and modulus difference) occurred. As such, the strengthening observed in the specimen aged for 1000 min was also due to precipitate shear.

The increase in strength of the specimens aged for 100 and 1000 min was calculated as $\sigma_{ys(aged)} - \sigma_{ys(ST)} - \Delta\sigma_{ss}$ accounting for the loss in solid solution strengthening. These data, plotted in Fig. 5a, b using green symbols, was within 10% of the calculated precipitation strengthening using models for shear mechanism. Thereby, strengthening due to precipitate shear had a significant contribution to the overall yield strength for specimens aged for 100 and 1000 min. In summary, calculations using well-established models for precipitation strengthening showed that shearing of the κ -carbide precipitates was the predominant mechanism for strengthening in specimens aged for 100 and 1000 min.

4 Conclusions

The low density austenitic steel (Fe–0.8C–31.52Mn–8.73Al) was subjected to aging treatment and the microstructure and mechanical properties were characterized. Thermodynamic

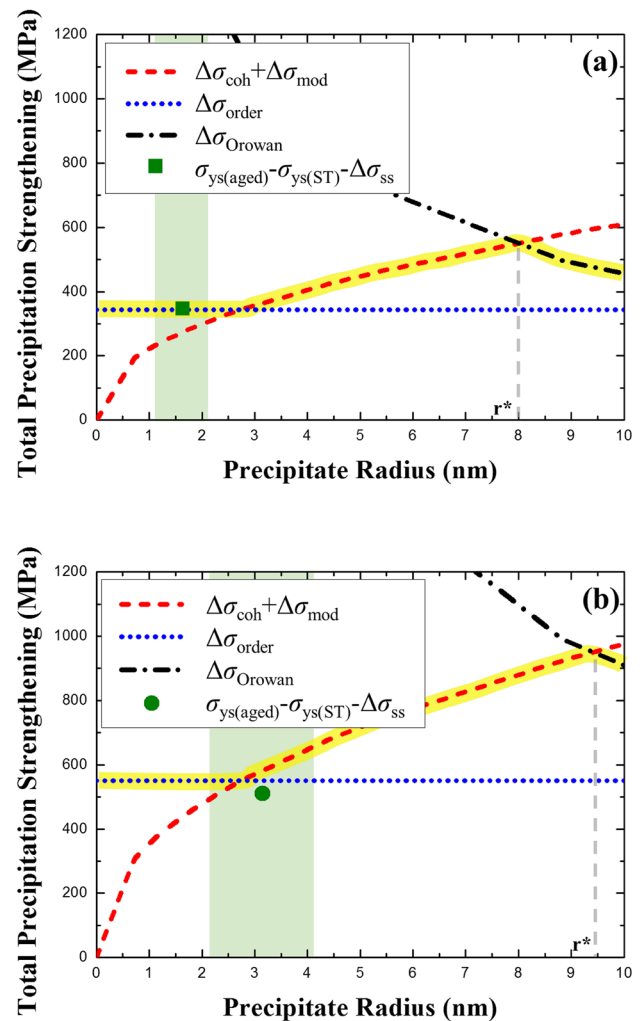


Fig. 5 Increase in yield strength as a function of precipitate mean radius **a** calculated using κ -carbide phase fraction of 0.054 after 100 min of aging, and **b** calculated using κ -carbide phase fraction of 0.137 after 1000 min of aging. The region shaded in green indicates the precipitate radius measured using TEM. The highlighted yellow line indicates the operative mechanism for each radius. (Color figure online)

(ThermoCalc) and thermo-kinetic (MatCalc) simulations were carried out to determine equilibrium phase fractions and simulate the aging treatment, respectively. Precipitation strengthening was analyzed using models based on different mechanisms and compared with the measured values. The following conclusions were drawn from this study.

1. The strength of the aged specimens increased with increasing aging time, without significant loss in ductility. After 1000 min of aging, the yield strength increased 93% while the elongation decreased only 25%.

2. The κ -carbide precipitate size and phase fraction predicted from thermo-kinetic simulations were in good agreement with the measured values.
3. The strengthening in specimens aged for both 100 and 1000 min was mainly due to precipitate shearing.
4. The average multiplication factor of 0.64 approximated the precipitation strengthening adequately.

Acknowledgements This work was supported by the Materials and Components Technology Development Program (10048157) funded by the Ministry of Trade, Industry and Energy (MOTIE, Korea), and the National Research Foundation of Korea (NRF) grant funded by the Ministry of Science, ICT & Future Planning (MSIP) (No. NRF-2015R1A5A1037627). The Institute of Engineering Research at Seoul National University provided research facilities for this work.

References

1. I. Kalashnikov, A. Shalkevich, O. Acselrad, L.C. Pereira, *J. Mater. Eng. Perform.* **9**, 597 (2000)
2. G. Frommeyer, U. Brüx, *Steel Res. Int.* **77**, 627 (2006)
3. J.D. Yoo, K.-T. Park, *Mater. Sci. Eng. A* **496**, 417 (2008)
4. R.A. Howell, D.C. Van Aken, *AIST* **6**, 193 (2009)
5. G. Frommeyer, M. Bausch, RFCS Technical Group TGS7 Meeting (2013)
6. H. Kim, D.-W. Suh, N.J. Kim, *Sci. Tech. Adv. Mater.* **14**, 014205 (2013)
7. S.-J. Park, B. Hwang, K. Lee, T.-H. Lee, D.-W. Suh, H. Han, *Scr. Mater.* **68**, 365 (2013)
8. D.W. Suh, N.J. Kim, *Scr. Mater.* **68**, 337 (2013)
9. R. Rana, *JOM* **66**, 1730 (2014)
10. D. Raabe, H. Springer, I. Gutiérrez-Urrutia, F. Roters, M. Bausch, J.-B. Seol, M. Koyama, P.-P. Choi, K. Tszuzaki, *JOM* **66**, 1845 (2014)
11. P.D. Nezhadfar, A. Zarei-Hanzaki, S.S. Sohn, H.R. Abedi, *Met. Mater. Int.* **22**, 810 (2016)
12. H. Ding, D. Han, J. Zhang, Z. Cai, Z. Wu, M. Cai, *Mater. Sci. Eng. A* **652**, 69 (2016)
13. R. Rana, C. Liu, R.K. Ray, *Scr. Mater.* **68**, 354 (2013)
14. S.S. Sohn, B.J. Lee, S. Lee, N.J. Kim, J.H. Kwak, *Acta Mater.* **61**, 5050 (2013)
15. S.S. Sohn, H. Song, B.-C. Suh, J.-H. Kwak, B.-J. Lee, N.J. Kim, S. Lee, *Acta Mater.* **96**, 310 (2015)
16. K. Choi, C.-H. Seo, H. Lee, S.K. Kim, J.H. Kwak, K.G. Chin, K.-T. Park, N.J. Kim, *Scr. Mater.* **63**, 1028 (2010)
17. I. Gutierrez-Urrutia, D. Raabe, *Scr. Mater.* **68**, 343 (2013)
18. C.-L. Lin, C.-G. Chao, J.-Y. Juang, J.-M. Yang, T.-F. Liu, *J. Alloys Compd.* **586**, 616 (2014)
19. H. Springer, D. Raabe, *Acta Mater.* **60**, 4950 (2012)
20. W.K. Choo, J.H. Kim, J.C. Yoon, *Acta Mater.* **45**, 4877 (1997)
21. K. Sato, K. Tagawa, Y. Inoue, *Mater. Sci. Eng. A* **111**, 45 (1989)
22. K. Lee, S.-J. Park, J. Moon, J.-Y. Kang, T.-H. Lee, H.N. Han, *Scr. Mater.* **124**, 193 (2016)
23. K. Lee, S.-J. Park, J. Lee, J. Moon, J.-Y. Kang, D.-I. Kim, J.-Y. Suh, H.N. Han, *J. Alloys Compd.* **656**, 805 (2016)
24. J. Moon, S.-J. Park, J.H. Jang, T.-H. Lee, C.-H. Lee, H.-U. Hong, D.-W. Suh, S.H. Kim, H.N. Han, B.H. Lee, *Scr. Mater.* **127**, 97 (2017)
25. K. Lee, S.-J. Park, Y.S. Choi, S.-J. Kim, T.-H. Lee, K.H. Oh, H.N. Han, *Scr. Mater.* **69**, 618 (2013)
26. S.-J. Park, Y.-U. Heo, Y.H. Choi, K. Lee, H.N. Han, D.-W. Suh, *JOM* **66**, 1837 (2014)
27. K. Lee, S.-J. Park, J.-Y. Kang, S. Park, S.S. Han, J.Y. Park, K.H. Oh, S. Lee, A.D. Rollett, H.N. Han, *J. Alloys Compd.* **723**, 146 (2017)
28. J. Moon, S.-J. Park, C. Lee, H.N. Han, T.-H. Lee, C.-H. Lee, *Metall. Mater. Trans. A* **48**, 4500 (2017)
29. J.-H. Lee, S.-J. Park, J. Moon, J.-Y. Kang, J.-Y. Park, T.-H. Lee, K.M. Cho, *Korean J. Met. Mater.* **55**, 363 (2017)
30. P. James, *J. Iron Steel Inst.* **207**, 54 (1969)
31. G.L. Kayak, *Met. Sci. Heat Treat.* **11**, 95 (1969)
32. C.N. Hwang, C.Y. Chao, T.F. Liu, *Scr. Metall. Mater.* **28**, 263 (1993)
33. I. Gutierrez-Urrutia, D. Raabe, *Mater. Sci. Tech.* **30**, 1099 (2014)
34. C.W. Kim, S.I. Kwon, B.H. Lee, J.O. Moon, S.J. Park, J.H. Lee, H.U. Hong, *Mater. Sci. Eng. A* **673**, 108 (2016)
35. J.-H. Shim, E. Kozeschnik, W.-S. Jung, S.-C. Lee, D.-I. Kim, J.-Y. Suh, Y.-S. Lee, Y.W. Cho, *Calphad* **34**, 105 (2010)
36. Y.-S. Ji, J. Park, S.-Y. Lee, J.-W. Kim, S.-M. Lee, J. Nam, B. Hwang, J.-Y. Suh, J.-H. Shim, *Mater. Charact.* **128**, 23 (2017)
37. I. Holzer, E. Kozeschnik, *Mater. Sci. Eng. A Struct.* **527**, 3546 (2010)
38. E. Povoden-Karadeniz, E. Kozeschnik, *ISIJ Int.* **52**, 610 (2012)
39. K.-G. Chin, H.-J. Lee, J.-H. Kwak, J.-Y. Kang, B.-J. Lee, *J. Alloys Compd.* **505**, 217 (2010)
40. E. Kozeschnik, J. Svoboda, F.D. Fischer, *Calphad* **28**, 379 (2004)
41. E. Kozeschnik, J. Svoboda, P. Fratzl, F.D. Fischer, *Mater. Sci. Eng. A* **385**, 157 (2004)
42. B. Lee, B. Sundman, *TCFE2000: The Thermo-Calc Steels Database* (KTH, Stockholm, 1999)
43. V. Ragavan, *Materials Science and Engineering, First Course* (Prentice-Hall, India, 1985)
44. R. Labusch, *Acta Metall.* **20**, 917 (1972)
45. U. Kocks, A.S. Argon, M. Ashby, *Thermodynamics and Kinetics of Slip* (Argonne National Laboratory, Lemont, 1973)
46. C. Varvenne, G. Leyson, M. Ghazisaeidi, W. Curtin, *Acta Mater.* **124**, 660 (2017)
47. P. Kusakin, A. Belyakov, D.A. Molodov, R. Kaibyshev, *Mater. Sci. Eng. A* **687**, 82 (2017)
48. A. Ardell, *Metall. Trans. A* **16**, 2131 (1985)
49. M. Meyers, *Mechanical Metallurgy: Principles and Applications* (Prentice-Hall Inc, Englewood Cliffs, 1984)
50. J.W. Martin, *Precipitation Hardening: Theory and Applications* (Butterworth-Heinemann, Oxford, 2012)
51. D.N. Seidman, E.A. Marquis, D.C. Dunand, *Acta Mater.* **50**, 4021 (2002)
52. L. Brown, R. Ham, in *Strengthening Mechanisms in Crystals*, ed. by A. Kelly, R.B. Nicholson (Elsevier, Amsterdam, 1971)
53. P. Hirsch, F. Humphreys, in *The Physics and Strength of Plasticity*, ed. by A. Argon (MIT Press, Cambridge, 1969)
54. E. Nembach, *Particle Strengthening of Metals and Alloys* (Wiley, New York, 1997)
55. L. Bartlett, A.M. Schulte, D.C. Van Aken, K.D. Peaslee, R.A. Howell, *Mater. Sci. Technol.* **2010**, 1941–1953 (2010)